coatings

MDPI

Article

Influence of Surface Roughness and Agitation on the Morphology of Magnetite Films Electrodeposited on Carbon Steel Substrates

Soon-Hyeok Jeon, Won-Ik Choi, Geun-Dong Song, Yeong-Ho Son and Do Haeng Hur *

Nuclear Materials Safety Reserach Division, Korea Atomic Energy Research Institute, Daejeon 305-353, Korea; junsoon@kaeri.re.kr (S.-H.J.); wonik134@kaeri.re.kr (W.-I.C.); sgd84@kaeri.re.kr (G.-D.S.); syhm0907@kaeri.re.kr (Y.-H.S.)

* Correspondence: dhhur@kaeri.re.kr; Tel.: +82-42-868-8696

Academic Editor: Giovanni Zangari

Received: 29 August 2016; Accepted: 14 November 2016; Published: 16 November 2016

Abstract: In this work, we investigated the effects of surface roughness and agitation on the morphology of magnetite films electrodeposited from alkaline Fe(III)-triethanolamine (TEA) solutions on carbon steel substrates. The surface roughness of the carbon steel substrates was maintained in the range of 1.64–0.06 μm by using mechanical grinding and polishing methods. The agitation speed was set at 0 and 900 rpm during the electrodeposition process. The particle size and surface roughness value of the magnetite films gradually decreased with decreasing substrate roughness. However, the influence of the substrate roughness on the thickness of the magnetite film was negligible. The morphology of the magnetite film fabricated at 900 rpm appeared to be highly faceted compared to that of the magnetite film produced at 0 rpm. The thickness and surface roughness of the magnetite film significantly increased with the agitation speed, which also significantly affected the electrodeposition efficiency. The effects of substrate surface roughness and agitation on the morphology of magnetite films electrodeposited on carbon steel substrates were also discussed. The obtained results provide critical information for the simulation of magnetite deposits on carbon steel pipes in the secondary systems of nuclear power plants.

Keywords: magnetite; electrodeposition; surface roughness; agitation; morphology

1. Introduction

Magnetite is a half-metallic metal oxide with inverse spinel structure and cubic lattice parameter, a = 0.8397 nm (space group = Fd3m); it exhibits ferrimagnetism below the Curie temperature of 860 K [1,2]. The tetrahedral sites are occupied by Fe^{3+} ions, while the octahedral sites are shared by Fe^{3+} and Fe^{2+} ions. Ferrimagnetism results from the presence of Fe atoms in two different redox states and their positioning in the crystal structure.

In nuclear power plants, magnetite is well known as a major corrosion by-product, as it forms on the surface of carbon steel pipes of the secondary coolant systems of nuclear pressurized water reactors (PWR) [3,4]. Wall thinning of carbon steel pipes, vessels, and tubes is generally caused by flow accelerated corrosion (FAC), which is caused by the removal of the magnetite layer in a stream of flowing water or wet steam. FAC has caused a large number of failures in carbon steel pipelines of PWR secondary circuits [4].

The formation of magnetite on carbon steel piping of PWR secondary circuits has attracted considerable interest because wall thinning leads to sudden pipe rupture, unless it is detected on time and the piping is replaced [5]. Since the first piping rupture at Trojan in 1985, about 270 carbon steel piping wall thinning records have been reported for PWRs from 1995 [6]. More recently, in 2004, a pipe rupture accident occurred in the proximity of a flow-meter [7]. Aside from the wall thinning problem

due to FAC, the corrosion rate of carbon steel piping with magnetite formation increases because magnetite is electrically contacted with carbon steel, resulting in a galvanic effect between the two materials [8,9].

To investigate the various corrosion behaviors of carbon steel piping due to magnetite formation in secondary systems of nuclear power plants, such as FAC and galvanic corrosion, a valid method of depositing magnetite on carbon steel substrates should be established. Therefore, it is of high interest to find a simple and efficient technique for the production of magnetite films.

Several methods based on electrodeposition have been studied [10–16]. There are two basic approaches to depositing pure magnetite; i.e., by anodic deposition in Fe(II) systems [10–12], and cathodic deposition in Fe(III) systems [13–16]. In the former method, Fe(II) ions were complexed with acetate anions and electrochemically oxidized to form a magnetite film in an inert atmosphere at elevated temperatures. A disadvantage of this method is that complexed Fe(II) can be oxidized by molecular oxygen in air; thus, special treatment must be conducted to remove molecular oxygen.

To solve this problem, Sapieszko and Matijevic [14] proposed the cathodic reduction of Fe(III) complexed with triethanolamine (TEA) to produce pure magnetite by hydrothermal method. This technique was further used by Tarascon's group to fabricate magnetite electrodes for Li ion batteries [15,16]. Recently, Switzer and co-workers modified the Fe(III)–TEA solution agent and developed an efficient method to produce pure magnetite on stainless steel substrate [17], single crystal Au substrate [18], or Ni substrate [19]. In this modified method, the elimination of molecular oxygen from the deposition bath is not necessary, owing to the good stability of the Fe(III)–TEA complex [18–20]. Goujon et al. [20,21] studied the structures of iron oxide films electrodeposited on the Ni-based super alloys (Inconel 600 and 690) at varying electrodeposition potentials. Notably, optimal electrodeposition conditions were established to produce thick and dense pure-magnetite films in Fe(III)–TEA solution. Duan et al. [22] conducted a systematic study on the critical factors affecting magnetite deposition in Fe(III)–TEA solutions, such as concentration of Fe(III) ion, deposition temperature, and time. The Fe(III) ion concentration had an impact on the deposition rate, while the deposition temperature and time strongly affected the morphology of the magnetite films.

However, until now, no systematic study on the factors affecting magnetite deposition in Fe(III)–TEA systems—such as substrate surface roughness and agitation speed—has been reported. Especially, the effects of substrate surface roughness and agitation speed on the morphology, thickness, and surface roughness of magnetite films deposited on carbon steel substrates have not been investigated.

In this paper, we reported a systematic investigation of the morphology of magnetite films deposited on carbon steel substrates from Fe(III)–TEA solutions, with particular regard to the substrate surface roughness and agitation speed during the electrodeposition process. This work can provide useful information for the simulation of magnetite deposits on carbon steel piping, vessels, and tubing in the secondary systems of nuclear power plants.

2. Materials and Methods

Carbon steel specimens were machined into 10 mm × 5 mm × 1 mm from the SA106Gr.B pipe material. The specimens were ground with silicon carbide (SiC) papers of up to #80, #220, #600, and #2000 grit by using a rotating polishing machine. All specimens were ultrasonically cleaned in ethanol for 5 min. Finally, specimens with four different surface states were prepared. The chemical composition of carbon steel is given in Table 1.

The magnetite films were electrodeposited from an alkaline solution of $Fe_2(SO_4)_3$ complexed with TEA. The concentrations in the electrodeposition bath were 0.09 M $Fe_2(SO_4)_3$, 0.1 M TEA, and 2 M NaOH. The deposition solution was prepared by slowly adding and dissolving $Fe_2(SO_4)_3$ in water to a stirred solution of NaOH and TEA. The resulting electrodeposition solution was gray-green colored with pH 12.5 at 25 °C. The resulting gray-green solution was heated to 80 °C and stirred at 200 rpm.

Table 1. Chemical composition of the carbon steel substrate (wt.%).

Composition	wt.%	Composition	wt.%
C	0.19	Cu	0.1
Cr	0.4	Mn	1.05
Ni	0.2	S	0.005
Mo	0.1	P	0.012
Si	0.23	Fe	Bal.

Figure 1 shows a schematic of the electrodeposition apparatus. The electrochemical deposition of magnetite on carbon steel substrate was conducted using a three electrode cell and a potentiostat. A saturated calomel electrode (SCE) and a platinum wire were used as the reference and counter electrode, respectively. During the electrodeposition process, the solution was maintained at 80 °C. Magnetite films were electrodeposited at −1.05 V_{SCE} for 1800 s with and without stirring at 900 rpm. To compare the morphologies of the same thick magnetite films with and without stirring at 900 rpm, magnetite films were also electrodeposited at −1.05 V_{SCE} with stirring at 900 rpm for 700 s. As a result, magnetite films with almost same thickness were produced.

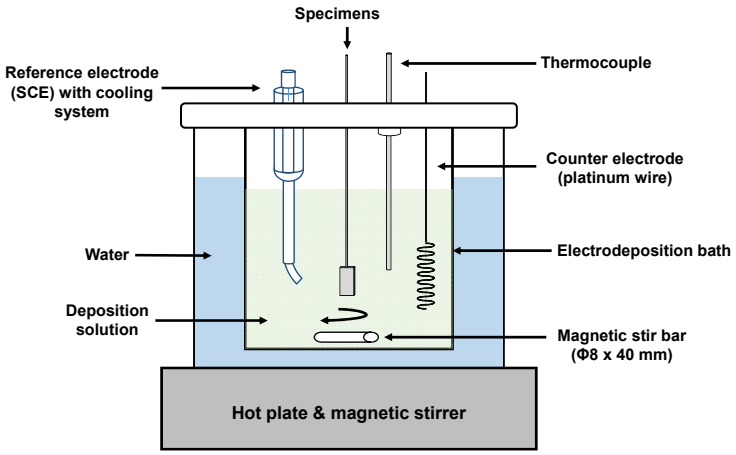

Figure 1. Schematic of electrodeposition apparatus. SCE: saturated calomel electrode.

Stirring of the deposition solution was carried out using a magnetic stirrer and cylindrical shaped magnetic stir bar (Φ 8 × 40 mm). To ensure an electrodeposition that was as homogeneous as possible, the carbon steel specimens were fixed in front of the counter electrode. After the electrodeposition, the magnetite films were carefully rinsed with deionized water and dried in air.

In order to analyze the morphology and thickness of the magnetite films deposited on carbon steel substrates, the magnetite films were analyzed by scanning electron microscope (SEM). Adherence of magnetite films was confirmed by SEM. Crystallinity of magnetite films was analyzed by X-ray diffraction (XRD). The surface roughness values of substrate and magnetite were measured using a non-contacting surface profiler. The measurement areas for surface roughness values of substrate and magnetite films were about 0.618 mm^2. In this paper, the root mean square roughness (R_q) was used as a roughness parameter. The thickness and roughness of magnetite films were measured at least three times to confirm the reproducibility. The values are presented as the average with error bars, and good reproducibility was confirmed.

3. Results

3.1. Electrodeposition of Magnetite Films

Figure 2 shows the R_q of the specimens as measured using a non-contacting surface profiler. The surface roughness value of the specimen polished with #80 grit SiC paper was the highest (1.64 μm).

The surface roughness values gradually decreased with increasing SiC grit size. The specimen polished with #2000 grit paper showed the lowest roughness value of 0.06 μm.

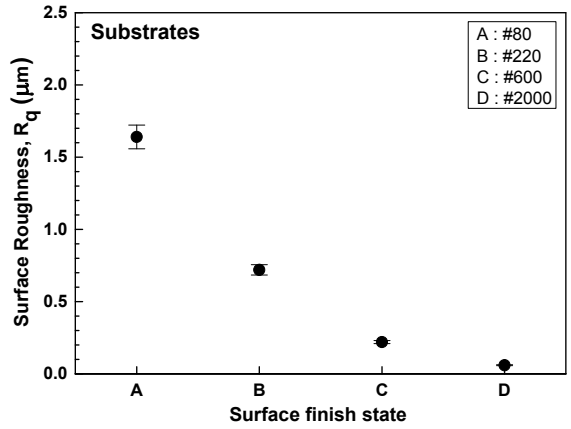

Figure 2. Surface roughness values of carbon steel substrates at different surface finish states.

Figure 3 shows a linear sweep voltammogram of the carbon steel substrate polished with #600 grit paper in Fe(III)–TEA solution at 80 °C. The potential was swept from the open circuit potential to −1.25 V_{SCE} at the scan rate of 5 mV/s. The electrochemical reduction of Fe(III)–TEA started at potentials more negative than −0.95 V_{SCE}. The first reduction wave of the linear sweep was measured approximately between −0.95 and −1.20 V_{SCE}. The second reduction wave was observed in the potential range between −1.20 and −1.25 V_{SCE}.

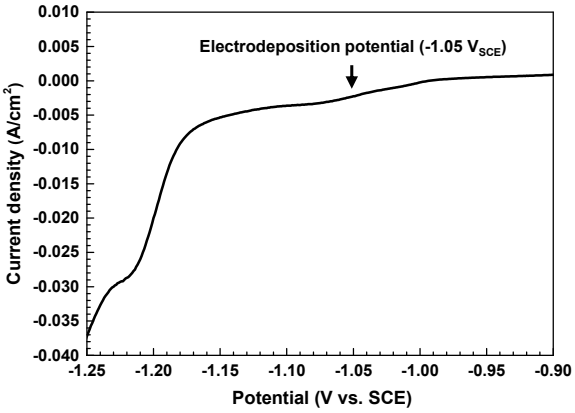

Figure 3. Linear sweep voltammogram of carbon steel substrate in Fe(III)–triethanolamine (TEA) solution at 80 °C.

The electrodeposition of a magnetite film from an Fe(III)–TEA solution can be divided into two distinct processes. The first process entails the electrochemical reduction of the Fe(III)–TEA solution to an Fe(II)-TEA complex, as described by Reaction (1). The second process involves the chemical reaction of the Fe(III)–TEA complex with Fe(II)-TEA to produce a magnetite film on the surface of the carbon steel substrate in the following Reaction (2). Reaction (3) describes the overall electrochemical reaction leading to the formation of the magnetite film [17–19].

$$Fe(OH)_4TEA_2^- + e^- \rightarrow Fe(TEA)_2^{2+} + 4OH^- \quad (1)$$

$$2Fe(OH)_4TEA_2^- + Fe(TEA)_2^{2+} \leftrightarrow Fe_3O_4 + 6TEA + 4H_2O \quad (2)$$

$$3Fe(OH)_4TEA_2^- + e^- \rightarrow Fe_3O_4 + 6TEA + 4H_2O + 4OH^- \quad (3)$$

The first reduction wave observed between −0.95 and −1.20 V_{SCE} can be attributed to a one-electron reaction corresponding to Reaction (1) [18]. Conversely, the second reduction wave between −1.20 and −1.25 V_{SCE} seems to be due to a two-electron process corresponding to the reduction of Fe(II) to Fe [18,19]. In this work, magnetite films were electrodeposited on carbon steel substrates of various surface roughnesses and at different agitation speeds of Fe(III)–TEA solutions at 80 °C. Magnetite was deposited at the potential of −1.05 V_{SCE} (first reduction wave region) for 700 s and 1800 s.

Figure 4 shows the variation of electrodeposition current density at various surface roughnesses and agitation speeds during the electrodeposition process. The current density of the magnetite films remained almost constant over the surface roughness range of 1.64–0.06 μm. However, it significantly increased with the agitation speed.

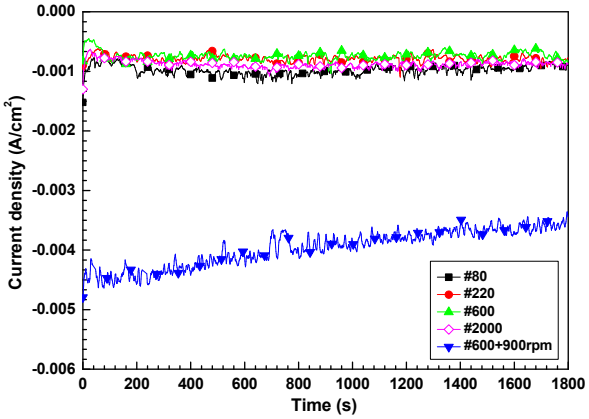

Figure 4. Current density variation with different roughnesses and agitation speeds during electrodeposition at −1.05 V_{SCE} in Fe(III)–TEA solution at 80 °C.

3.2. Morphology of the Magnetite Films

Figure 5 shows the surface morphologies of magnetite films formed at different substrate surface roughnesses and agitation speeds during electrodeposition; clearly, both of these factors affected the film morphology. The particle size of the magnetite films gradually decreased with decreasing substrate roughness from 1.64 to 0.06 μm.

The change in the particle size of the electrodeposited magnetite film with the substrate roughness can be explained on the basis of two important factors. First, it can be related to the change of the diffusion zone according to the roughness of the substrate. During the electrodeposition process, substrates with different surface roughnesses provide different diffusion zones. On a substrate with a smooth surface, the diffusion zone is relatively homogeneous over the whole substrate surface [23–26]. Thus, the concentration gradient of the depositing species between the bulk solutions and the substrate–solution interface follows a linear concentration profile across the whole substrate surface by diffusion. When performing electrodeposition on a smooth substrate, the homogeneous diffusion zone can lead to the formation of a relatively fine-grained deposition layer [23,27]. However, the situation is completely different on a rough substrate. The diffusion zone converges at peak of rough surface [23,24,28]. This convergent diffusion, which results in faster mass transport per unit area of the rough substrate, contributes to the nucleation. When nucleation on a rough substrate occurs, the growth of nuclei and the diffusion of depositing species converge at the peak of the rough surface, disappearing nuclei around the peak [23,27]. Second, the change in magnetite particle size with the substrate roughness is related to the frequency of the nucleation. Commonly, the surface energy of a rough substrate is higher than that of a smooth substrate, as the surface area increases with the substrate roughness [29,30]. In addition, the nucleation rate is lower on substrates with higher surface energy [30]. Thus, the nucleation rate of magnetite on carbon steel substrate decreased with increasing substrate surface roughness. Namely, a smooth substrate with relatively low surface energy

promotes a high degree of nucleation, resulting in the formation of an electrodeposited magnetite layer with a fine-grained structure. For these reasons, the electrodeposited particle size is increased with increasing surface roughness of the substrate.

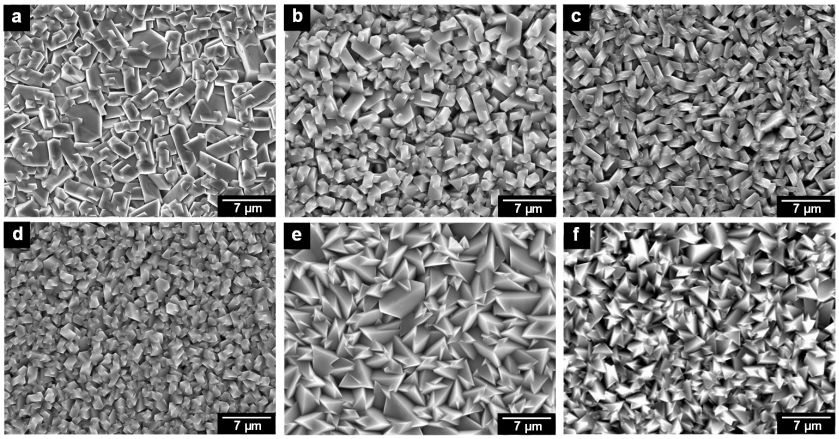

Figure 5. Scanning electron microscopy (SEM) images of the surface of magnetite films on carbon steel substrates with different roughnesses and agitation speeds at the -1.05 V_{SCE} in Fe(III)–TEA solution at 80 °C: (**a**) #80 grit, (**b**) #220 grit, (**c**) #600 grit, (**d**) #2000 grit, (**e**) #600 grit + stirring 900 rpm, and (**f**) #600 grit + stirring 900 rpm (deposition time: 700 s).

For the substrate polished with #600 grit SiC paper, both magnetite films formed at 900 rpm for 700 s and 1800 s exhibited a highly faceted and dense morphology compared to those formed at 0 rpm. This result indicates that the morphology of the magnetite film is affected by the agitation speed, regardless of deposition time. However, the particle size of magnetite films formed at 900 rpm for 1800 s was larger than that of the films formed at 900 rpm for 700 s. Under the same deposition time, the effect of agitation on the morphology of magnetite deposits is due to the decrease of the thickness of the cathode diffusion layer and enhancement of ion mass transport to the carbon steel substrate. The increase of mass transport in the deposition solution results in a quick compensation of the depletion of ions in the vicinity of the substrate. Hence, the morphology is determined by the preferential growth of favorably-oriented crystal faces. As a result, the deposited magnetite film formed at 900 rpm assumed a dense morphology with tightly packed, well-faceted crystallites. In addition, the changes, due to agitation, in particle size and morphology of magnetite films on substrates having the same roughness can be explained considering the increase of deposition current by hydrogen formation. In the cathodic deposition process for the formation of magnetite from an Fe(III)–TEA solution, the electrochemical reaction at the substrate surface involves hydrogen evolution as well as reduction from ferrous iron to ferric iron. The increase in deposition current by agitation reveals higher hydrogen formation at the substrate surface. In this regard, it was reported that hydrogen reduced the surface energy of the substrate and promoted planar growth of electrodeposited particles [29,31]. For these reasons, stirring the deposition solution increases hydrogen evolution and facilitates the formation of a thick magnetite layer with larger particles. Kim et al. [32] studied the effect of stirring rate on the grain size of electrolessly-deposited Co–W–P thin films. The average grain size of the crystals linearly increased with increasing stirring rate of the electrolyte from 0 to 1300 rpm, owing to the increase in mass transport in the solution.

Figure 6 shows the cross-sectional SEM images of different magnetite films. Under all electrodeposition conditions, the magnetite films were very compact and adherent to the carbon steel substrate. No defects (such as holes, gaps, and cracks) could be observed at the interface between film and substrate, which confirmed that the deposited films were tightly bonded to the substrates. In addition, the influence of substrate roughness on the thickness of the magnetite film was negligible. On the other hand, the thickness sharply increased with the agitation speed under the same deposition

time. As shown in Figure 6f, the magnetite film deposited at −1.05 V_{SCE} with stirring at 900 rpm for 700 s was produced to almost same thickness, compared with those of magnetite films without stirring.

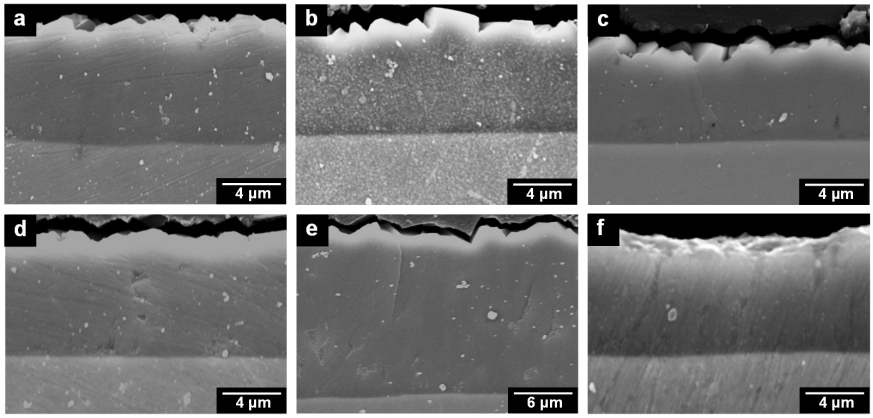

Figure 6. SEM images of the cross section of magnetite films on carbon steel substrates with different roughnesses and agitation speeds at the −1.05 V_{SCE} in Fe(III)–TEA solution at 80 °C: (**a**) #80 grit, (**b**) #220 grit, (**c**) #600 grit, (**d**) #2000 grit, (**e**) #600 grit + stirring 900 rpm, and (**f**) #600 grit + stirring 900 rpm (deposition time: 700 s).

Figure 7 shows the thickness variation of magnetite films prepared at various substrate roughnesses and agitation speeds. The thicknesses of the magnetite films were almost identical over the surface roughness range of 1.64–0.06 μm, indicating that the roughness negligibly affected the thickness. However, the thickness increased by about three times when the agitation speed increased under the same deposition time. As shown in Figure 4, the thickness of the magnetite film is strongly affected by the electrodeposition charge variation. The deposition rate could be determined by measuring the thickness of the deposit by a micrometer or by measuring the weight of the deposit. In this work, the deposition rate of the magnetite film dramatically increased with increasing agitation speed from 0 to 900 rpm, based on the thickness results. Some authors have studied the effects of agitation speed on film thickness and deposition rate [32,33]. The results showed that the deposition rate increased dramatically with the solution agitation. The thickness of the film deposited from a stagnant solution was 50 nm, while that of the film deposited under solution agitation of 1280 rpm was 92 nm. Bulasara et al. [33] investigated the variation of average nickel plating rate with the stirrer speed. The authors reported that the mass transfer enhancement in the form of membrane stirring caused about a 20%–56% increase in the average nickel deposition rate.

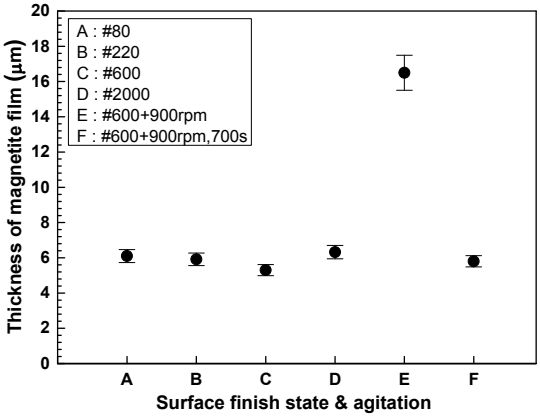

Figure 7. Thickness of the magnetite films on carbon steel substrates with different roughnesses and agitation speeds at −1.05 V_{SCE} in Fe(III)–TEA solution at 80 °C.

3.3. X-ray Diffraction of Magnetite Films

Figure 8 shows the XRD patterns of magnetite films deposited at various substrate roughnesses and agitation speeds. The electrodeposited magnetite films were all crystalline, and all peaks corresponded to those of magnetite (JCPDS card no. 19-0629), with the (311) reflection being the strongest. Among all reflections, the (440) reflection of the magnetite film at 0 rpm was relatively high over the surface roughness range of 1.64–0.06 μm. The (220) reflection of magnetite films with surface roughness of 1.64 μm was considerably more intense than that of magnetite films with surface roughnesses in the range of 0.72–0.06 μm. These results showed that the magnitude of the (220) reflection was affected from the variation in magnetite particle size. In the case of the magnetite film with a surface roughness value of 0.22 μm, the relative intensities of the XRD peaks of the film formed at 900 rpm were significantly different from those of the film formed at 0 rpm. The XRD relative intensity of the (220) reflection sharply increased, while that of the (440) reflection decreased. These changes in XRD intensity were closely related to the remarkable changes in particle morphology and size. During the electrodeposition process, the agitation increases the mass transport in the deposition solution, which results in a quick compensation of the depletion of ions in the vicinity of the substrate. Hence, the morphologies of the magnetite particles were modified by the preferential growth of favorably oriented crystal faces, and the particle size significantly increased. In a previous study, Inoue and Hirasawa [34] showed the relationship between XRD peak intensity and morphology on $CaSO_4 \cdot 2H_2O$ crystals synthesized by crystallization reaction with various additives. They reported that the XRD relative intensity increased when needle-like or plate-like large crystals were transformed into granular microcrystals. However, the intensities of the XRD peaks of the film formed at 900 rpm for 700 s was not significantly changed compared to those of the films at 0 rpm. This result is because there was no difference in magnetite particle size.

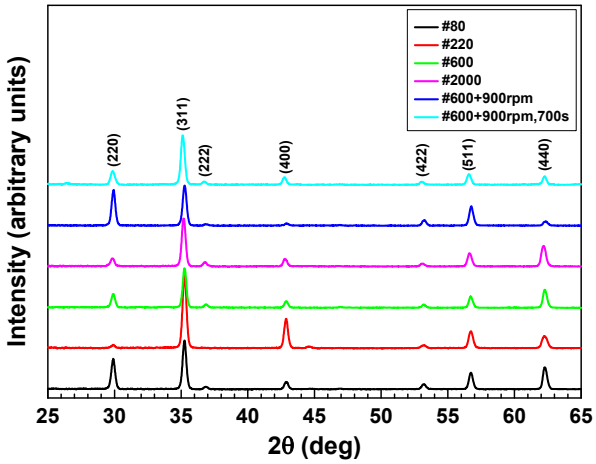

Figure 8. X-ray diffraction (XRD) patterns of the magnetite film on carbon steel substrates with different roughnesses and agitation speeds at −1.05 V_{SCE} in Fe(III)–TEA solution at 80 °C.

3.4. Surface Roughness of Magnetite Films

Figure 9 shows the three-dimensional (3D) surface roughness of magnetite films on carbon steel substrates deposited at various substrate roughnesses and agitation speeds, as measured by the use of a non-contact surface profiler. The film roughness depended on the substrate surface roughness and morphology, as shown in Figures 1 and 5. The roughness gradually decreased with decreasing surface roughness of the specimens from 1.64 to 0.06 μm, owing to the decrease in magnetite particle size. The sharp increase in roughness at 900 rpm was due to the highly faceted morphology of the magnetite film. The roughness of the film formed at 900 rpm for 700 s is not significant changed, compared with that of the films at 0 rpm. This result is because there is no difference in magnetite particle size.

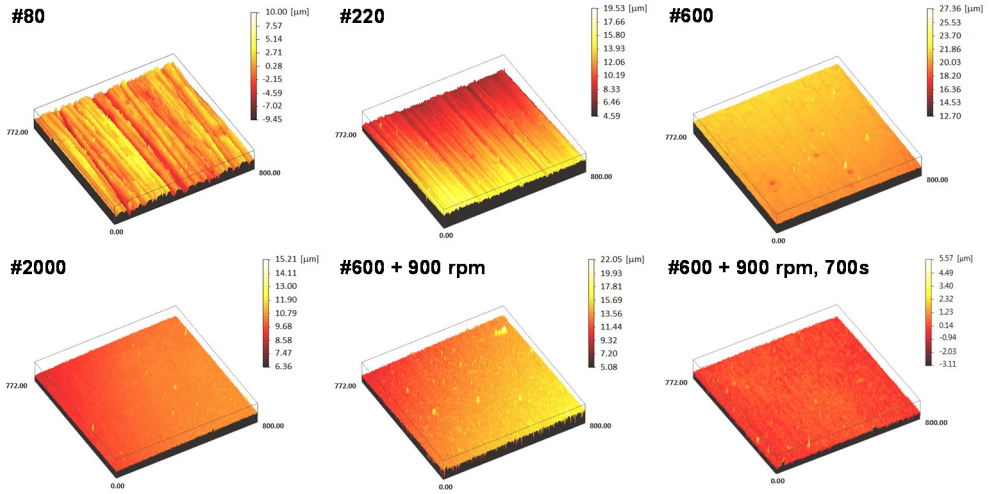

Figure 9. 3D surface roughness profile of magnetite films on carbon steel substrates with different roughnesses and agitation speeds.

Figure 10 shows the R_q values of the magnetite films obtained from 3D surface roughness profiles. The surface roughness of the magnetite film ground to #2000 grit was 0.22 μm. These results showed that the magnetite film surface roughness was considerably affected by the substrate surface roughness.

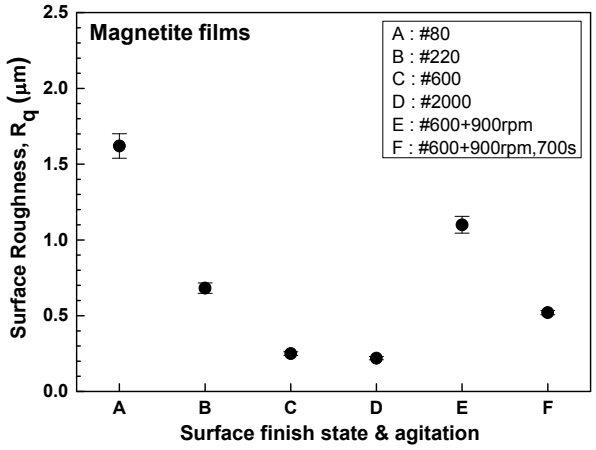

Figure 10. Surface roughness of magnetite films on carbon steel substrates with different roughnesses and agitation speeds.

In this work, we investigated the dependence of morphology and thickness of magnetite films on the substrate surface roughness and agitation speed. The obtained results showed that the morphology of the magnetite film could be significantly controlled by altering the substrate surface roughness and agitation speed. In addition, the deposition rate increased with increasing agitation speed. These results are crucial to facilitate the attainment of the desired morphologies and thicknesses in magnetite films. This work also provides relevant information for the simulation of magnetite deposits on carbon steel piping, vessels, and tubing in the secondary systems of nuclear power plants.

Notably, in the secondary systems of nuclear power plants, porous magnetite is the main corrosion product formed on the surface of carbon steel piping, steam generator tubing, and other support structures. Tapping et al. [35] reported that the thickness of porous magnetite on carbon steel piping, steam generator (SG) tubing, and other SG support structures exceeds several tens of micrometers in nuclear power plants. The morphology of magnetite deposits could be varied depending on the operation time and water chemistry conditions such as dissolved oxygen, dissolved hydrogen,

temperature, and pH. Although the electrodeposited magnetite films do not have a porous structure like real corrosion products, they could be used as specimens for electrochemical tests, as they appear compact and firmly adherent to the carbon steel substrate. Furthermore, no defects such as holes, gaps, and cracks could be observed at the interface between magnetite films and carbon steel substrates, which confirmed that the deposited magnetite films were tightly bonded to the substrates. Hence, magnetite films electrodeposited on carbon steel substrates could be used to investigate various corrosion behaviors, such as FAC and galvanic corrosion of magnetite deposited on carbon steel and reductive dissolution of magnetite in PWR secondary systems.

4. Conclusions

In this work, we reported a systematic investigation of the morphology of magnetite films deposited on carbon steel substrates from Fe(III)–TEA solutions, with particular regard to the substrate surface roughness and agitation speed during the electrodeposition process. The substrate surface roughness and agitation speed affected the morphology, thickness, and surface roughness of the magnetite films. The particle size and surface roughness value of the magnetite films gradually decreased with decreasing the substrate roughness. However, the influence of the substrate roughness on the thickness of the magnetite film was negligible. The morphology of the magnetite film fabricated at 900 rpm appeared to be highly faceted compared to that of the magnetite film produced at 0 rpm. The thickness and surface roughness of the magnetite film significantly increased with the agitation speed, which also significantly affected the electrodeposition efficiency. These results are crucial to facilitate the attainment of the desired morphologies and thicknesses in magnetite films. Besides, this work provides relevant information for the simulation of magnetite deposits on carbon steel piping, vessels, and tubing in the secondary systems of nuclear power plants.

Acknowledgments: This work was supported by the National Research Foundation of Korea (NRF) grant funded by the Korea government (MSIP) (2012M2A8A4025888).

Author Contributions: Soon-Hyeok Jeon and Do Haeng Hur conceived, designed the experiments and wrote the paper; Won-Ik Choi and Yeong-Ho Son performed the experiments; Geun-Dong Song analyzed the data.

Conflicts of Interest: The authors declare no conflict of interest. The sponsor had no role in the design of the study; in the collection, analyses or interpretation of data; in the writing of the manuscript, or in the decision to publish the results.

References

1. Verwey, E.J.W. Electronic conduction of magnetite (Fe_3O_4) and its transition point at low temperature. *Nature* **1939**, *144*, 327–328. [CrossRef]
2. Walz, F. The Verwey transition-a topical review. *J. Phys. Condens. Matter* **2002**, *14*, R285–R340. [CrossRef]
3. Burrill, K.A.; Cheluget, E.L. Corrosion of CANDU Outlet Feeder Pipes. In Proceedings of the International Conference on Water Chemistry in Nuclear Power Plants, Nigata, Japan, 13–16 October 1998.
4. Cook, W.G.; Lister, D.H. Some Aspects of Electrochemistry and Corrosion Mechanisms Influencing Flow Assisted Corrosion in CANDU Outlet Feeder Pipes. In Proceedings of the International Conference on Water Chemistry of Nuclear Reactor Systems, San Francisco, CA, USA, 11–14 October 2004.
5. Jung, K.S.; Sung, K.W. Magnetite: Electrochemical Properties and Its Role on Flow Accelerated Corrosion. In *Magnetite: Structure, Properties and Applications*; Nova Science Publishers: New York, NY, USA, 2010; pp. 261–298.
6. Shah, V.N. Flow-Accelerated Corrosion of PWR Carbon Steel Components. Presented at Symposium on Life Extension and Aging Management of Nuclear Power Plant Components in Korea, Taejon, Korea, July 1999.
7. Accident at the Kansai Electric's Mihama-3 NPS. JAIF Focus, Japan Atomic Industrial Forum, Inc.: Tokyo, Japan, 2004.
8. Jeon, S.H.; Song, G.D.; Hur, D.H. Electrodeposition of magnetite on carbon steel in Fe(III)-triethanolamine solution and its corrosion behavior. *Mater. Trans.* **2015**, *56*, 1107–1111. [CrossRef]

9. Song, G.D.; Jeon, S.H.; Hur, D.H. Effect of polyacrylic acid on the corrosion behavior of carbon steel and magnetite in alkaline aqueous solutions. *Corrosion* **2016**, *72*, 1010–1020. [CrossRef]
10. Carlier, D.; Terrier, C.; Arm, C.; Anserment, J.P. Preparation and magnetic properties of Fe_3O_4 nanostructures grown by electrodeposition. *Electrochem. Solid State Lett.* **2005**, *8*, 43–46. [CrossRef]
11. Peulon, S.; Antony, H.; Legrand, L.; Chausse, A. Thin layers of iron corrosion products electrochemically deposited on inert substrates: synthesis and behavior. *Electrochim. Acta* **2004**, *49*, 2891–2899. [CrossRef]
12. Wang, S.Y.; Ho, K.C.; Kuo, S.L.; Wu, N.L. Investigation on capacitance mechanisms of Fe_3O_4 electrochemical capacitors. *Electrochem. Soc.* **2006**, *153*, A75–A80. [CrossRef]
13. Teng, C.L.; Ryan, M.P. A morphological study of nanocrystalline magnetite electrodeposited onto polycrystalline copper substrates. *Electrochem. Solid State Lett.* **2007**, *10*, D108–D112. [CrossRef]
14. Sapieszko, R.S.; Matijevic, E. Preparation of well-defined colloidal particles by thermal decomposition of metal chelates. I. Iron oxides. *J. Colloid Interface Sci.* **1980**, *74*, 405–422. [CrossRef]
15. Mitra, S.; Poizot, P.; Finke, A.; Tarascon, J.M. Growth and electrochemical characterization versus lithium of Fe_3O_4 electrodes made by electrodeposition. *Adv. Funct. Mater.* **2006**, *16*, 2281–2287. [CrossRef]
16. Taberna, P.L.; Mitra, S.; Poizit, P.; Tarascon, J.M. High rate capabilities Fe_3O_4-based Cu nano-architectured electrodes for lithium-ion battery applications. *Net. Mater.* **2006**, *5*, 567–573. [CrossRef] [PubMed]
17. Kothari, H.M.; Kulp, E.A.; Limmer, S.J.; Poizot, P.; Bohannan, E.W.; Switzer, J.A. Electrochemical deposition and characterization of Fe_3O_4 films produced by the reduction of Fe(III)-triethanolamine. *J. Mater. Res.* **2006**, *21*, 293–301. [CrossRef]
18. Kulp, E.A.; Kothari, H.M.; Limmer, S.J.; Yang, J.; Gudavarthy, R.V.; Bohannan, E.W.; Switzer, J.A. Electrodeposition of epitaxial magnetite films and ferrihydritenanoribbons on single-crystal gold. *Chem. Mater.* **2009**, *21*, 5022–5031. [CrossRef]
19. Gudavarthy, R.V.; Gorantla, S.; Mu, G.; Kulp, E.A.; Gemming, T.; Eckert, J.; Switzer, J.A. Epitaxial electrodeposition of Fe_3O_4 on single-crystal Ni(111). *Chem. Mater.* **2011**, *23*, 2017–2019. [CrossRef]
20. Goujon, C.; Pauporté, T.; Mansour, C.; Delaunary, S.; Bretelle, J.L. Fouling of Steam Generator Tubes in Nuclear Power Plants: Laboratory Tests to Reproduce Oxides Deposition. In Proceedings of the International Conference on Heat Exchanger Fouling and Cleaning, Budapest, Hungary, 9–14 June 2013; pp. 101–107.
21. Goujon, C.; Pauporté, T.; Mansour, C.; Delaunary, S.; Bretelle, J.L. Electrochemical deposition of thick iron oxide films on nickel based superalloy substrates. *Electrochim. Acta* **2015**, *176*, 230–239. [CrossRef]
22. Duan, H.; Chen, X.; Li, B.; Liang, J. Growth morphology study of cathodically electrodeposited Fe_3O_4thin films at elevated temperatures. *Mater. Res. Bull.* **2010**, *45*, 1696–1702. [CrossRef]
23. Huang, X.J.; Yarimaga, O.; Kim, J.H.; Choi, Y.K. Substrate surface roughness-dependent 3-D complex nanoarchitectures of gold particles from directed electrodeposition. *J. Mater. Chem.* **2009**, *19*, 478–483. [CrossRef]
24. Gunawardena, G.; Hills, G.; Montenegrom, I.; Scharifker, B. Electrochemical nucleation: Part I. General considerations. *J. Electroanal. Chem.* **1982**, *138*, 225–239. [CrossRef]
25. Leopoldes, J.; Damman, P. From a two-dimensional chemical pattern to a three-dimensional topology through selective inversion of a liquid-liquid bilayer. *Nat. Mater.* **2006**, *5*, 957–961. [CrossRef] [PubMed]
26. Squires, T.M.; Quake, S.R. Microfluidics: Fluid physics at the nanoliter scale. *Rev. Mod. Phys.* **2005**, *77*, 977–1026. [CrossRef]
27. Castro-Rodriguez, R.; Oliva, A.I.; Sosa, V.; Caballero-Briones, F.; Pena, J.L. Effect of indium tin oxide substrate roughness on the morphology, structural and optical properties of CdS thin films. *Appl. Surf. Sci.* **2000**, *161*, 340–346. [CrossRef]
28. Depestel, L.M.; Strubbe, K. Electrodeposition of gold from cyanide dolution on different n-GaAs crystal faces. *J. Electroanal. Chem.* **2004**, *572*, 195–201. [CrossRef]
29. Ebrahimi, F.; Ahmed, Z. The effect of current density on properties of electrodeposited nanocrystalline nockel. *J. Appl. Electrochem.* **2003**, *33*, 733–739. [CrossRef]
30. Zamanzad-Ghavidel, M.R.; Raeissi, K.; Saatchi, A. Effect of substrate texture and deposition current density on properties of Ni nanocrystalline electrodeposition. *Iran. J. Mater. Sci. Eng.* **2012**, *9*, 1–14.
31. Haug, K.; Jenkins, T. Effect of Hydrogen on the Three-Dimensional Epitaxial Growth of Ni(100), (110), and (111). *J. Phys. Chem. B* **2000**, *104*, 10017–10023. [CrossRef]
32. Kim, T.H.; Dulal, S.M.S.I.; Park, C.H.; Chae, H.; Kim, C.K. Optimisation of process parameters for electroless plating of Co-W-P capping layers from an alkali-metal-free bath. *Surf. Coat. Technol.* **2008**, *202*, 4861–4867. [CrossRef]

33. Bulasara, V.K.; Thakuria, H.; Uppaluri, R.; Purkait, M.K. Combination performance characteristics of agitated nickel hypophosphite electroless plating baths. *J. Mater. Proc. Technol.* **2011**, *211*, 1488–1499. [CrossRef]
34. Inoue, M.; Hirasawa, I. The relationship between crystal morphology and XRD peak intensity on $CaSO_4 \cdot 2H_2O$. *J. Cryst. Growth* **2013**, *380*, 169–175. [CrossRef]
35. Tapping, R.L.; Turner, C.W.; Thompson, R.H. Steam generator deposits-a detailed analysis and some inferences. *Corrosion* **1991**, *47*, 489–495. [CrossRef]